Journal of Sound and Vibration 325 (2009) 722–741

Contents lists available at ScienceDirect

Journal of Sound and Vibration

journal homepage: www.elsevier.com/locate/jsvi

Comparison of external damping models in a large deformation problem

Jae Wook Lee [1], Hyun Woo Kim [1], Hi Chun Ku [1], Wan Suk Yoo *

School of Mechanical Engineering, Pusan National University, Busan 609-735, South Korea

ARTICLE INFO

Article history:
Received 5 October 2008
Received in revised form
19 March 2009
Accepted 8 April 2009
Handling Editor: J. Lam
Available online 30 May 2009

ABSTRACT

In many applications of flexible multibody dynamics, the magnitudes of damping forces are very small in comparison with the elastic and inertial forces. However, these small forces may have a very significant influence on responses near resonant frequencies. The role of damping is to remove the energy of a system by dissipation, and dissipative forces in structures can be the result of either internal or external damping. External damping includes aerodynamic and hydrodynamic drag and dissipation in the supports of structures, and internal damping is usually related to energy dissipation in materials.

In large deformation problems, because of the flexibility of very thin structures, external damping is more important. Two types of damping models, proportional damping and quadratic damping, have been widely applied to flexible multibody dynamics. The advantages and weaknesses of the two damping models are considered in this study. To make up for the common drawbacks in these two models, a frequency-dependent generic damping model based on experimental modal analysis is proposed. The proposed damping model leads to a accurate correlation with experimental results because it directly uses the modal parameters of each mode obtained by experiment, and can represent exact high frequency behaviors simultaneously. To define and formulate a large deformation problem, the absolute nodal coordinate formulation (ANCF) was used, and computer simulations with the ANCF were compared to experimental results. Using the proposed experimental method, modal parameters and damping behaviors are extracted until 5th mode, which has a frequency of 89 Hz. It is shown that the common drawbacks of proportional and quadratic damping are complemented by the proposed generic damping model.

1. Introduction

In many applications of flexible multibody dynamics, the magnitudes of damping forces are very small in comparison with the elastic and inertial forces. However, these small forces may have a very significant influence on response amplitude and phase near resonance. Damping removes energy in a system by dissipation, and dissipative forces in structures come from either internal or external damping. External damping includes aerodynamic and hydrodynamic drag and dissipation in the supports of structures, and internal damping usually comes from energy dissipation between materials [1–5]. In general, the damping ratio must be determined experimentally because it depends on the amplitudes

* Corresponding author. Tel.: +82 51 510 2328; fax: +82 51 512 9835.
E-mail addresses: jaewk@hanmail.net (J.W. Lee), nectar78@empal.com (H.W. Kim), lunaticwar@naver.com (H.C. Ku), wsyoo@pusan.ac.kr (W.S. Yoo).
[1] Tel.: +82 51 510 1457; fax: +82 51 581 8514.

0022-460X/$ - see front matter © 2009 Elsevier Ltd. All rights reserved.
doi:10.1016/j.jsv.2009.04.018

and frequencies of the oscillating structure. Although an exact internal damping model can be developed by using the difficult viscoelastic theory, it must be correlated with experiment results if the mechanism does not operate in vacuum circumference. That is the reason why most field engineers consider it difficult to identify and analyze damping in real situations.

Damping is especially important in multibody dynamic simulation. The absolute nodal coordinate formulation (ANCF) [6,7] is widely used to explain the large deformations of flexible structures, because it defines displacements and slopes from a global inertial frame. Because this formulation was developed quite recently, very few related studies on damping exist. Most researchers use traditional Rayleigh proportional damping for the sake of simplicity. Takahashi et al. [8] introduced a Rayleigh proportional damping matrix using the assumption that deformations within each finite element are small. Yoo et al. [9] used a proportional damping approach to model external damping, and checked their results against experimental data. They found good consistency, even with large oscillations, in a cantilever beam; however, they focused only on first mode behavior. To correlate the fundamental mode, proportional damping is sufficient, because two control parameters can give good results for the first mode. Moreover, to explain only the fundamental frequency, one control parameter is sufficient. Thus, they concluded that the mass proportional damping model is sufficient to explain the motion of the large oscillation. However, the proportional damping model has a critical intrinsic weakness: it is impossible to correlate high frequency behavior with just two control parameters. Yoo et al. [10] also used a quadratic damping model to represent the strong air influence effects on a thin plate. The quadratic damping model could be applied to the immersed model with a large drag coefficient, but this model cannot control the various mode behaviors at the same time. Garcia-Vallejo [11] suggested an internal damping model based on linear visco elasticity for the ANCF. He made a damping model which allowed no energy dissipation under rigid body motion; this was an effective approach for structural dynamics as well as flexible multibody dynamics simulation. However, because of thin structure in large deformation analysis, external damping is more important than internal damping in most mechanical applications except hyperelastic or viscoelastic materials. It is therefore necessary to find a new damping model which can express both internal and external damping characteristics, and can simultaneously explain high frequency behavior.

In this study, the characteristics of proportional damping and quadratic damping model are discussed and applied to flexible multibody dynamics. Since these two models cannot describe various frequency behaviors at the same time, a frequency-dependent generic damping model based on the experimental modal analysis is proposed [12,13]. The proposed model provides more accurate correlation results because it directly uses the modal parameters of each mode derived from experiments, and can present the exact high frequency behaviors simultaneously.

This paper is structured as follows: Section 2 describes the equations of motion for a two-dimensional (2-D) beam model with the ANCF. Section 3 describes our method of modal testing to correlate the ANCF simulation and to extract the modal parameters of the tested beam. Due to the flexibility of a very thin beam for which the fundamental frequency is only 1.85 Hz, traditional modal testing methods would not work well. Thus, a new experimental modal testing method is presented using a high speed camera to extract the modal parameters up to the 5th mode at 89 Hz. Section 4 describes the characteristics of three damping models, and the parameter identification method of each damping model is explained. Section 5 compares ANCF simulation results and experimental results. Finally, conclusions are drawn and discussed in Section 6.

2. Equations of motion for 2-D beam model with ANCF

A finite element model of a 2-D Euler–Bernoulli beam is shown in Fig. 1. The center line is parameterized by the value $p = 0, \ldots, l$ where l is the initial length of the beam element. The vectors in the absolute nodal coordinate formulation consist of displacement vectors r_0, r_l and tangent slopes τ_0, τ_l which are all defined from the inertial reference frame [9,14]. Therefore, Eq. (1) is the vector of the absolute nodal coordinates of the beam:

$$\mathbf{e} = \{r_0 \;\; \tau_0 \;\; r_l \;\; \tau_l\}^{\mathrm{T}} = \{e_1 \;\; e_2 \;\; e_3 \;\; e_4\}^{\mathrm{T}} \tag{1}$$

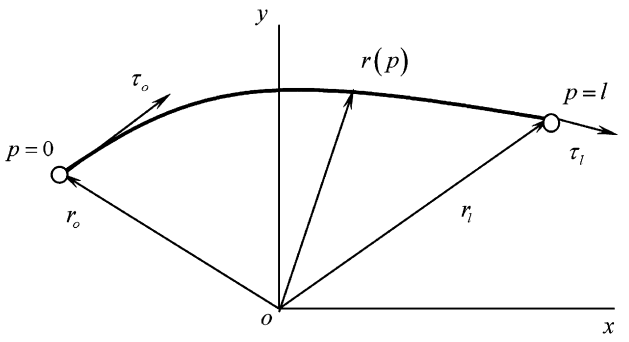

Fig. 1. Finite element of 2-D beam model.

It can be shown that the position of an arbitrary point on the element is given by

$$\mathbf{r}(p)=\mathbf{Se}=\begin{bmatrix} s_1 & 0 & s_2 & 0 & s_3 & 0 & s_4 & 0 \\ 0 & s_1 & 0 & s_2 & 0 & s_3 & 0 & s_4 \end{bmatrix}\begin{Bmatrix} \begin{Bmatrix} r_{0x} \\ r_{0y} \end{Bmatrix} \\ \vdots \\ \begin{Bmatrix} \tau_{lx} \\ \tau_{ly} \end{Bmatrix} \end{Bmatrix} \tag{2}$$

In Eq. (2), a global shape function is defined as shown in

$$s_1=1-3\xi^2+2\xi^3,\quad s_2=l(\xi-2\xi^2+\xi^3),\quad s_3=3\xi^2-2\xi^3,\quad s_4=l(\xi^3-\xi^2) \tag{3}$$

where $\xi=p/l$ is a non-dimensional variable.

The equations of motion of the beam element can typically be obtained using methods of analytical mechanics such as those based on Lagrange equations [9]. Thus,

$$\frac{\mathrm{d}}{\mathrm{d}t}\left(\frac{\partial T}{\partial \dot{\mathbf{e}}}\right)^{\mathrm{T}}-\left(\frac{\partial T}{\partial \mathbf{e}}\right)^{\mathrm{T}}+\left(\frac{\partial U}{\partial \mathbf{e}}\right)^{\mathrm{T}}=\left(\frac{\delta W}{\delta \mathbf{e}}\right)^{\mathrm{T}} \tag{4}$$

$$T=\frac{1}{2}\int_0^l \mu\dot{\mathbf{r}}^{\mathrm{T}}\dot{\mathbf{r}}\,\mathrm{d}p$$

$$\delta W=\int_0^l \delta\mathbf{r}^{\mathrm{T}}\mu\mathbf{g}\,\mathrm{d}p \tag{5}$$

where T is the kinetic energy, U is the strain energy by internal force, δW is the virtual work of external forces, and μ is the linear mass density.

After substituting Eqs. (2) and (5) into Eq. (4), we rearrange the equation in matrix form as follows:

$$\mathbf{M}\ddot{\mathbf{e}}+\mathbf{Q}^e=\mathbf{Q}^g \tag{6}$$

where

$$\mathbf{M}_{ij}=\frac{\partial^2 T}{\partial\dot{\mathbf{e}}_i\partial\dot{\mathbf{e}}_j^{\mathrm{T}}}=\underbrace{\mu\int_0^l s_i s_j\,\mathrm{d}p}_{M_{ij}}\mathbf{I}=M_{ij}\mathbf{I}$$

$$\mathbf{Q}_i^g=\frac{\delta W}{\delta\mathbf{e}_i}=\mu\mathbf{g}\int_0^l s_i\,\mathrm{d}p,\quad i,j=1,\ldots,4 \tag{7}$$

The block element of the mass matrix and the vectors of generalized gravity forces are denoted by $\mathbf{M}_{ij}$ and $\mathbf{Q}_i^g$, respectively. Calculating the vectors of generalized elastic forces is very cumbersome because of the complexity of the strain energy term U. Thus, the strain energy is divided into tensile and flexural components as shown in

$$U=U^{\varepsilon}+U^{\kappa}=\frac{1}{2}\int_0^l EA\varepsilon^2\,\mathrm{d}p+\frac{1}{2}\int_0^l EI\kappa^2\,\mathrm{d}p \tag{8}$$

where ε represents the longitudinal deformation and κ represents the transverse curvature. The tensile stiffness EA and the flexural stiffness EI are assumed to be constant throughout the beam element. A more detailed derivation for the equations of motion and several models of elastic forces are given in Refs. [9,14].

3. Experimental modal testing and identification

In this study, we selected a thin spring-steel beam which was heat-treated to increase its strength and durability. The sectional properties of the selected beam with rectangular shape are shown in Table 1. Because of the flexibility of very thin beam, the fundamental frequency is only 1.85 Hz, traditional modal testing methods do not work well. Contact-type accelerometers have problems of mass cancellation, and non-contact-type accelerometers cannot guarantee a constant measuring point due to the large oscillation. Moreover, an impact hammer cannot be applied to such a very flexible

Table 1
Standard properties of the beam.

Length (mm)	Width (mm)	Thickness (mm)	Density (kg m^{-3})	Elastic modulus (MPa)
500	5.0	0.50	8000.0	210,000

structure because of double hammering and non-impactive force. Thus, it is difficult to trust the test results of traditional modal testing and, for a large oscillation or deformation test, another test procedure is required. In this study, a damped decay test of a clamped beam was measured with a high speed camera as shown in Fig. 2. The beam was located in the vertical direction, and the clamped end was excited along the horizontal direction at its natural frequencies until steady state behavior occurred. When the beam reached steady-state, a sudden drop of the excitation made the beam vibrate with its natural properties.

A high-speed camera (REDLAKE Motion Scope 1000s) is used to capture the motion instead of accelerometers which eliminated the mass effects. The high-speed camera setup is shown in Fig. 2. One end of the beam was fixed with a clamping device. The vibration signal was generated by a LabVIEW program and transferred to a LMT-100 exciter (Ling Electronics) using a PXI 4461 board, as shown in Fig. 3. The exciter can vibrate to 2000 Hz. The large deformation experimental setup for the beam was constructed as shown in Fig. 4. A target point was required to track the beam position using the high speed camera.

Using this experiment setup, the displacements of the target point in the beam experiencing large oscillations were measured and are shown in Figs. 5–9. To find the modal parameter and damping ratio of the beam, a one degree of freedom (DOF) free vibration equation was used as follows:

$$r(t) = e^{-\zeta\omega_n t}\left(r_0\cos(\omega_d t) + \frac{\dot{r}_0 + \zeta\omega_n r_0}{\omega_d}\sin(\omega_d t)\right) \tag{9}$$

In Eq. (9), $\omega_d = \omega_n\sqrt{1-\zeta^2}$ is the damped natural frequency, ζ is damping ratio, and r_0 and $\dot{r}_0$ are the initial displacement and velocity of the measuring point of the beam, respectively. The modal parameters were calculated by

Fig. 2. High speed camera.

Fig. 3. PXI 4461 board (left) and exciter (right).

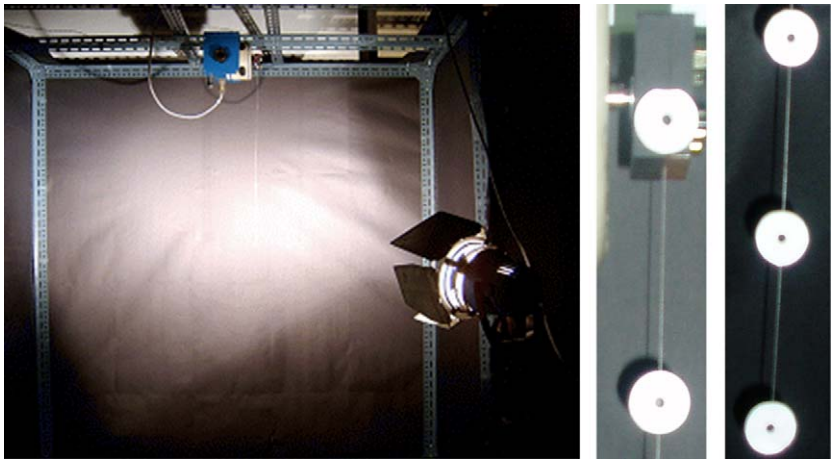

Fig. 4. Experimental setup and markers for tracking.

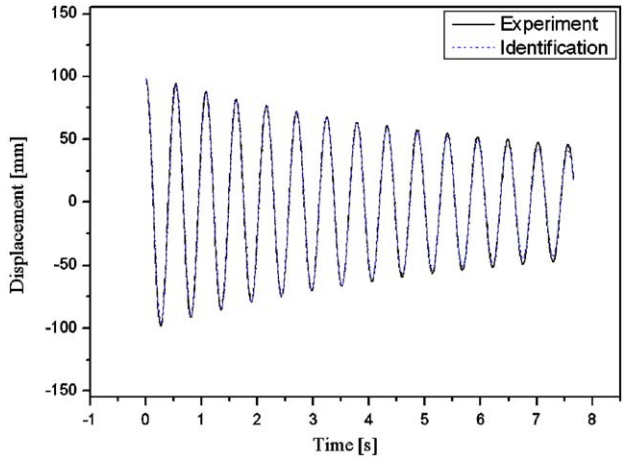

Fig. 5. Identification results of 1st mode: $\omega_1 = 1.85$ Hz and $\zeta_1 = 1.0$ percent.

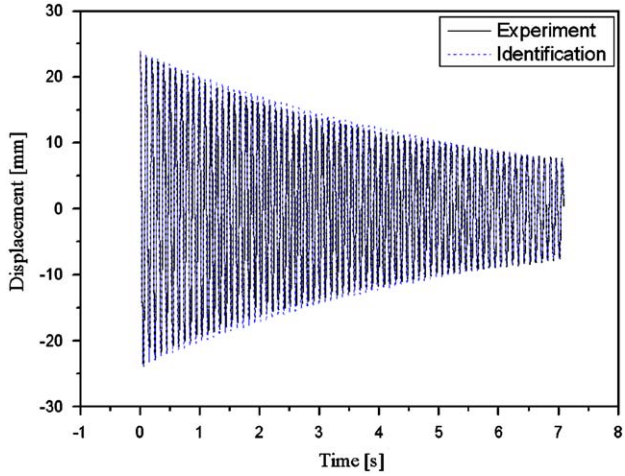

Fig. 6. Identification results of 2nd mode: $\omega_2 = 10.19$ Hz and $\zeta_2 = 0.28$ percent.

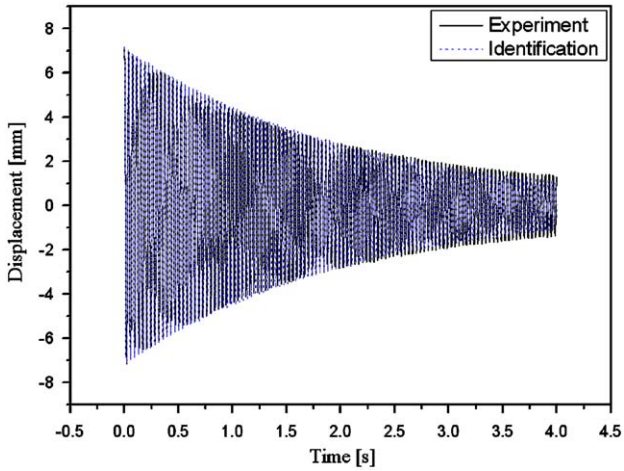

Fig. 7. Identification results of 3rd mode: $\omega_3 = 26.84$ Hz and $\zeta_3 = 0.28$ percent.

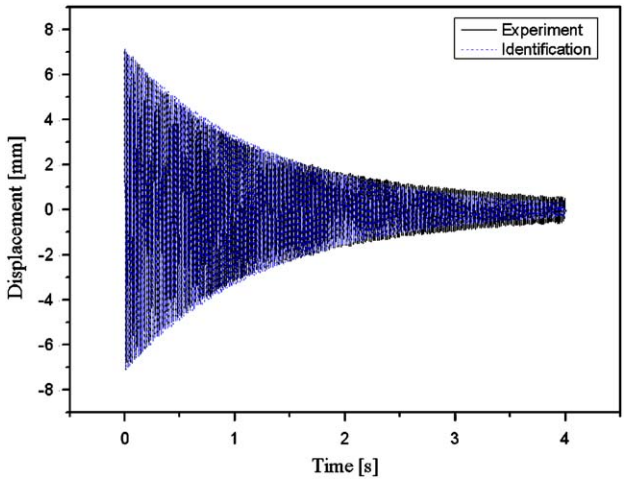

Fig. 8. Identification results of 4th mode: $\omega_4 = 53.20$ Hz and $\zeta_4 = 0.23$ percent.

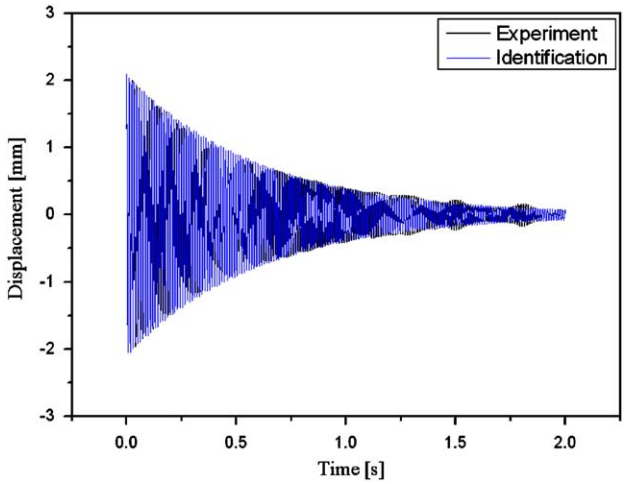

Fig. 9. Identification results of 5th mode: $\omega_5 = 88.60$ Hz and $\zeta_5 = 0.30$ percent.

Table 2
Identified modal parameters from experiments.

Mode	Natural frequency (Hz)	Damping ratio (%)
1st	1.85	1.00
2nd	10.19	0.28
3rd	26.84	0.28
4th	53.20	0.23
5th	88.60	0.30

minimizing the residue between experimentally obtained data and the ideal displacement such that

$$\text{Min.}\,\Re(\omega_n,\zeta_n)=\sqrt{\frac{1}{m}\sum_{i=1}^{m}(r_{\text{exp.}}-r_{\text{ide.}})^2} \tag{10}$$

Figs. 5–9 show the damping behavior of the beam from the 1st to the 5th natural frequency, respectively. In this figure, the "Experiment" (the black line) means the experimental results, and the "Identification" (the blue dashed line) means the curve fitting results from Eq. (9) with identified parameters. Table 2 shows the resultant modal parameters identified from the damping response of the beam.

4. External damping models in flexible multibody dynamics

4.1. Proportional damping model

To consider the effects of internal and external dissipation, the Rayleigh proportional damping model is widely used in structural dynamics for the sake of simplicity. In flexible multibody background, Takahashi et al. [8] and Yoo et al. [9] used this proportional damping model in their studies.

In general, viscous damping is proportional to the velocity of the system:

$$\mathbf{Q}^{\text{damp}}=\mathbf{C}\dot{r} \tag{11}$$

In the proportional damping model, there are various forms of damping, described by Eqs. (12)–(14), with various combinations of the mass and stiffness matrix:

$$\mathbf{C}_1=\alpha\mathbf{M} \tag{12}$$

$$\mathbf{C}_2=\beta\mathbf{K} \tag{13}$$

$$\mathbf{C}_3=\alpha\mathbf{M}+\beta\mathbf{K} \tag{14}$$

where **M** is a mass matrix and **K** is a stiffness matrix.

Expressions for the two control parameters can be derived as shown in

$$\ddot{r}_n+2\zeta_n\omega_n\dot{r}_n+\omega_n^2 r_n=0 \tag{15}$$

$$\zeta_n=\frac{\alpha+\beta\omega_n^2}{2\omega_n}=\frac{\alpha}{2\omega_n}+\frac{\beta\omega_n}{2} \tag{16}$$

$$\alpha=\frac{2\omega_1\omega_2(\zeta_1\omega_2-\zeta_2\omega_1)}{\omega_2^2-\omega_1^2},\quad \beta=\frac{2(\zeta_2\omega_2-\zeta_1\omega_1)}{\omega_2^2-\omega_1^2}\quad \text{for first two modes} \tag{17}$$

Values α, βdepend on frequencies ω_1 and ω_2 and on damping ratios ζ_1 and ζ_2 for first two modes of the system that appear in Eq. (17). The ratios ζ_1 and ζ_2 can be calculated from data identified in the previous section. Table 3 shows the resulting damping parameters calculated for computer simulations.

The proportional damping model is easy to use; however, its disadvantage is being able to control damping behavior with only two modes because there are only two constraint parameters, α and β. If the parameters were changed to correlate high frequency behavior, the low frequency motions would be different. In Eq. (17) and Fig. 10, we see that α controls low frequency behavior and β controls high frequency behavior. In Fig. 10, to depict these parameter characteristics, the relationship between excitation frequency and damping ratio is shown with arbitrary values ($\alpha=4.0$ and $\beta=0.1$).

In Ref. [9], the authors concluded that mass proportional damping as described by Eq. (12) was only necessity in large deformation analysis, and that stiffness proportional damping could be ignored in controlling large oscillation motion because the value of α was much greater than that of β. But, it was not true. Because they had focused on only 1st mode, the mass proportional damping is dominant in low frequency regions and the stiffness proportional damping can be ignored in

Table 3
Proportional damping parameters.

ω_1 (Hz)	ω_2 (Hz)	ζ_1 (%)	ζ_2 (%)	α	β
1.85	10.19	1.0	0.28	0.228	3.18E−4

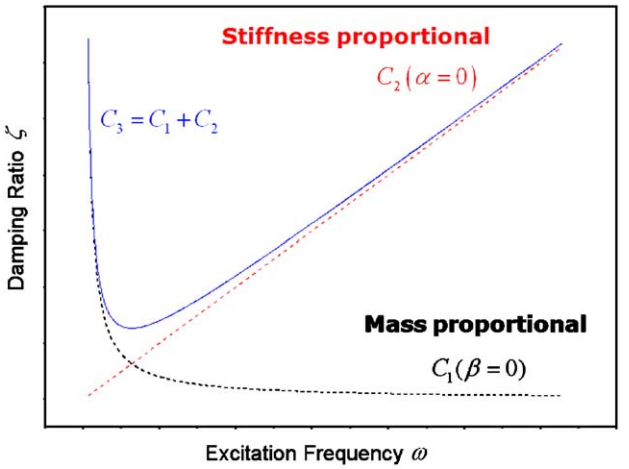

Fig. 10. Characteristic of several proportional damping models.

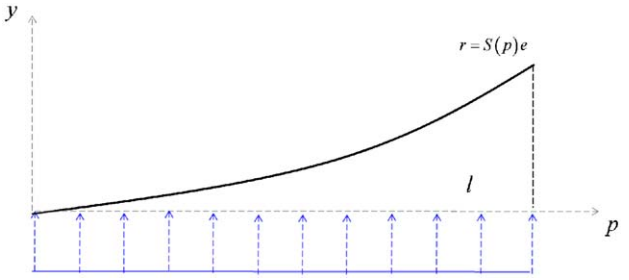

Fig. 11. Deflection mode of a cantilever beam under uniform loading.

their study. In the high frequency regions, the stiffness proportional damping is dominant as shown in Fig. 10. The stiffness proportional damping increased according to the increase in excitation frequency, so the proportional damping would tend predict the higher damping behavior in the high frequency regions.

4.2. Quadratic damping model

Linear damping cannot represent damping from hydrodynamic drag, which is a quadratic term. In Ref. [10], the significant influence of air resistance was applied to the vibration of a plate by adapting the quadratic term.

The external forces generated by fluid or hydrodynamic drag forces are generally expressed as shown in Ref. [15]

$$Q^{\text{damp}} = -\text{sgn}\left(\frac{\partial r}{\partial t}\right)\frac{1}{2}\rho_w C_d D f(t)\left|\frac{\partial r}{\partial t}\right|^2 \tag{18}$$

where ρ_w is the density of the fluid, C_d is the drag coefficient, D is the normal area of a flexible body and $f(t)$ is the loading function.

Similarly, assume that the damping force has linear and quadratic parts as follows:

$$\mathbf{Q}^{\text{damp}}(v) = \gamma_1 v + \gamma_2 v|v| \tag{19}$$

where unknown coefficients γ_1 and γ_2 are identified from experimental data.

Like Fig. 11, the assumed displacement and velocity field can be described by

$$r = r(p,e) = S(p)e$$

$$v = \dot{r}(p,\dot{e}) = S(p)\dot{e} \tag{20}$$

where $S(p)$ is the assumed deformation mode defined as

$$S(\xi) = \tfrac{1}{3}(6(\xi)^2 - 4(\xi)^3 + (\xi)^4) \tag{21}$$

The expression for the kinetic energy of the beam can be written as Eq. (22) with line mass density μ and a mass matrix $\mathbf{M}$:

$$T = \frac{1}{2}\mu\int_p S^2\dot{e}^2\,\mathrm{d}p = \frac{1}{2}\mathbf{M}\dot{e}^2 = \frac{1}{2}\left(\frac{104}{405}\mu a\right)\dot{e}^2 \tag{22}$$

The generalized damping force is given by

$$Q^{\mathrm{damp}} = \int_p Sq^{\mathrm{damp}}\,\mathrm{d}p = \int_p S(\gamma_1 S\dot{e} + \gamma_2 S\dot{e}|S\dot{e}|)\,\mathrm{d}p = \gamma_1\frac{1}{\mu}M\dot{e} + \gamma_2\left(\int_p S^2|S|\,\mathrm{d}p\right)\dot{e}|\dot{e}| \tag{23}$$

Since $S>0$ for $\forall p \in [0,l]$

$$\int_p S^2|S|\,\mathrm{d}p = \int_p S^3\,\mathrm{d}p = \frac{2336}{12,285}a \approx \frac{0.74}{\mu}M \tag{24}$$

Thus, if two auxiliary parameters are defined as shown in Eq. (25), the equation of motion of the beam with a quadratic damping model can be defined as shown in Eq. (26) in the case of a one DOF system.

$$\eta_1 = \frac{\gamma_1}{\mu}, \quad \eta_2 = \frac{0.74\gamma_2}{\mu} \tag{25}$$

$$M\ddot{e} + \eta_1 M\dot{e} + \eta_2 M\dot{e}|\dot{e}| + Ke = 0 \tag{26}$$

If the initial condition is $e(0) = e_0$, $\dot{e}(0) = 0$, the solution of Eq. (26) is given by [10]

$$e(t) \approx \frac{3\pi\eta_1 e_0 \exp^{-\eta_1 t/2}}{8\omega_n\eta_2 e_0(1-\mathrm{e}^{-\eta_1 t/2}) + 3\pi\eta_1}\cos\,\omega_n t \tag{27}$$

where 'exp' means the exponential function.

To identify parameters η_1 and η_2, the same identification process in Section 3 is fulfilled using Eq. (27) instead of Eq. (9). The resultant identified parameters are listed in Table 4.

The quadratic damping model is able to control two individual motions within one damping decay behavior with two control parameters. Namely, it is possible to express the air-resistance drag effects which are not proportional to the system velocity.

The characteristics of the quadratic damping model are shown in Figs. 12–15. To depict the effects of each quadratic parameter, the parameters are set up like Table 5. Quadratic 1 is linear damping in velocity ($\eta_1 = 2.0$, $\eta_2 = 0.0$) and Quadratic 2 means quadratic damping in velocity ($\eta_1 = 1.0\mathrm{E}{-9}$, $\eta_2 = 0.001$). Quadratic 1 is the same as the mass proportional damping in Eq. (12). Figs. 12 and 14 show that the damping decay motions are controlled by the combination of parameters η_1 and η_2. The η_1 model shows a more rapid decay response compared to the η_2 model.

As shown in Figs. 13 and 15, the η_1 model can control the residual oscillation after several seconds, because the vibration of the η_1 model disappeared after 5 s, but, the η_2 model oscillates for 15 s. Thus, we determine the frequency-dependent damping properties of the quadratic model. The η_1 model is independent of the excitation frequency but the η_2 model is strongly affected by excitation frequency. These characteristics of the quadratic damping parameter are summarized in Table 6.

Fig. 16 shows the influence of η_1 and η_2 on the quadratic damping during vibration decay. Both quadratic parameters and excitation frequency are listed in Table 7. The exponential decaying slope changed at 5 s according to the two quadratic parameters. Thus, the quadratic model can express the strong influence of air-resistance.

The drawback of the quadratic damping model is just to control damping behavior with only one mode even when using two control parameters. The number of simultaneously controlled modes is less than that of the proportional damping model. Thus, a different damping matrix at each mode is necessary to represent the damping motion of same mode, as shown in Table 4.

Table 4
Quadratic damping parameters and equivalent damping ratio.

Mode	ω (Hz)	η_1	η_2	ζ_{eq} (%)
1st	1.85	0.15	1.1E−4	1.00
2nd	10.19	0.31	6.0E−5	0.28
3rd	26.84	0.89	5.0E−5	0.28
4th	53.20	1.46	5.0E−5	0.23
5th	88.60	3.00	5.0E−5	0.30

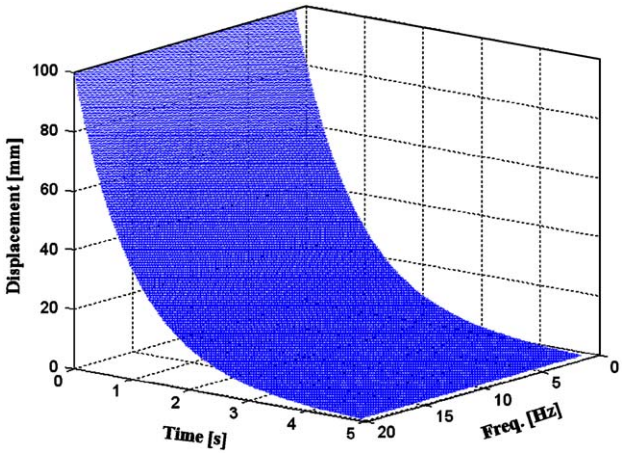

Fig. 12. Damping property of Quadratic 1 model: $\eta_1 = 2.0$ and $\eta_2 = 0.0$.

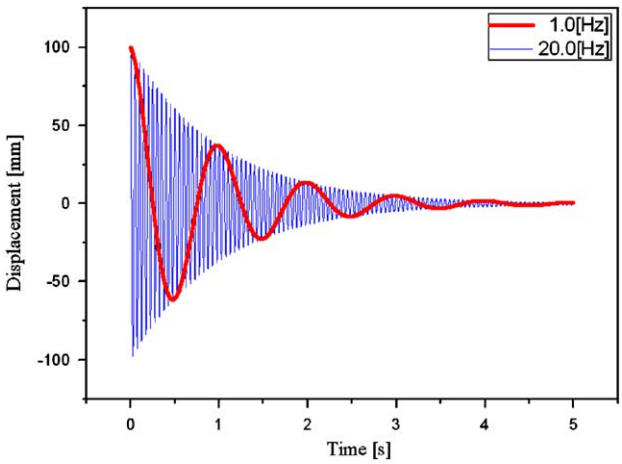

Fig. 13. Frequency independent property of Quadratic 1 model: $\eta_1 = 2.0$ and $\eta_2 = 0.0$.

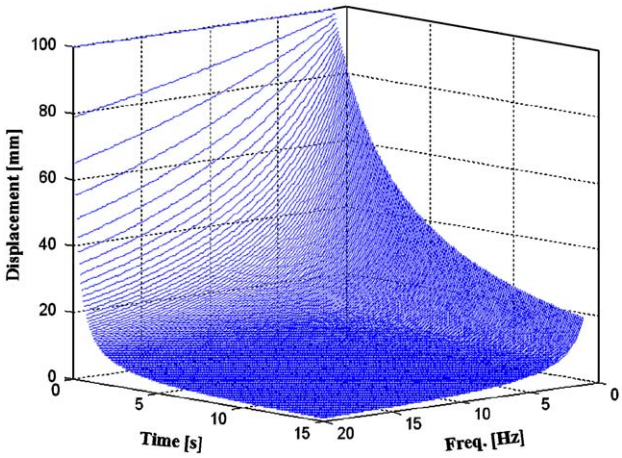

Fig. 14. Damping property of Quadratic 2 model: $\eta_1 = 1.0\text{E}{-9}$ and $\eta_2 = 0.0001$.

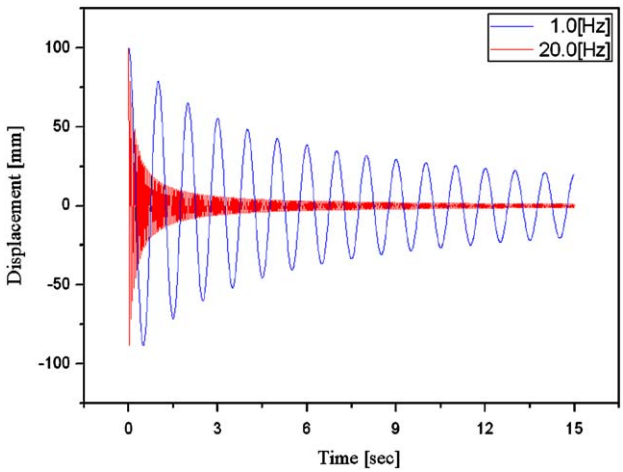

Fig. 15. Frequency dependent property of Quadratic 2 model: $\eta_1 = 1.0\text{E}{-9}$ and $\eta_2 = 0.001$.

Table 5
Quadratic damping parameters to check the characteristics of each parameter.

Quadratic	ω (Hz)	η_1	η_2
1	1.0–20.0	2.0	0.0
2	1.0–20.0	1.0E−9	0.001

Table 6
Characteristics of two quadratic parameters.

Quadratic	Gross motion	Frequency	Residual motion
1	Rapid decay	Independent	Controllable
2	Slow decay	Dependent	Uncontrollable

Table 7
Quadratic damping parameters to check the damping change during decaying.

Quadratic	ω (Hz)	η_1	η_2
3	1.85	1.5E−1	1.1E−4
4	1.85	3.0E−4	2.2E−4

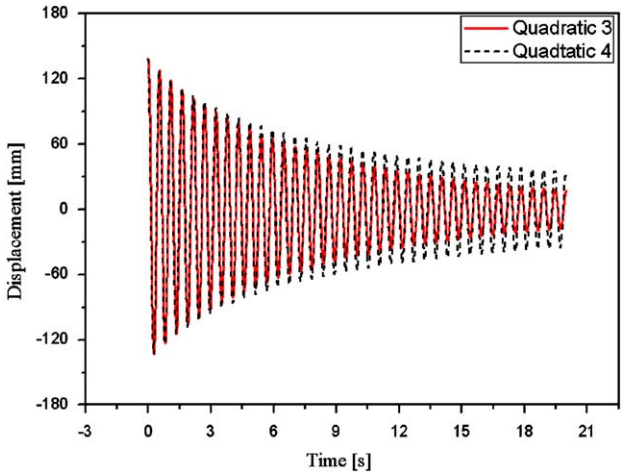

Fig. 16. Change of the damping ratio during decaying in quadratic damping; Quadratic 3 ($\eta_1 = 1.5\text{E}-1$, $\eta_2 = 1.1\text{E}-4$) and Quadratic 4 ($\eta_1 = 3.0\text{E}-4$, $\eta_2 = 2.2\text{E}-4$).

4.3. Generic damping model

In the previous section, it was shown that it is impossible to correlate the high frequency behavior of the structure using the proportional and quadratic damping model. The proportional model can control the motion of a maximum of two frequencies, and the quadratic damping model can control only one frequency behavior. Therefore, a new damping model which can have frequency dependent properties and can express the independent high frequency damping characteristic is necessary. In this study, a frequency dependent generic damping model based on experimental modal analysis is proposed and applied to the flexible multibody dynamics [12,13].

The generalized damping matrix can be derived from the identified modal parameters in Section 3. First, the modal superposition principal was used to stack up in the modal domain. Although the tested beam underwent large deformation, the amounts of the dissipated energy in each mode can be assumed to be independent of each other. Thus, linear superposition was applied and the inverse modal transformation can be applied under this assumption. Inverse modal

Table 8
Generic damping parameters to check the independent property w.r.t. neighboring damping ratio.

Generic	ζ_1 (%)	ζ_2 (%)
1	1.2	0.9
2	1.2	2.7

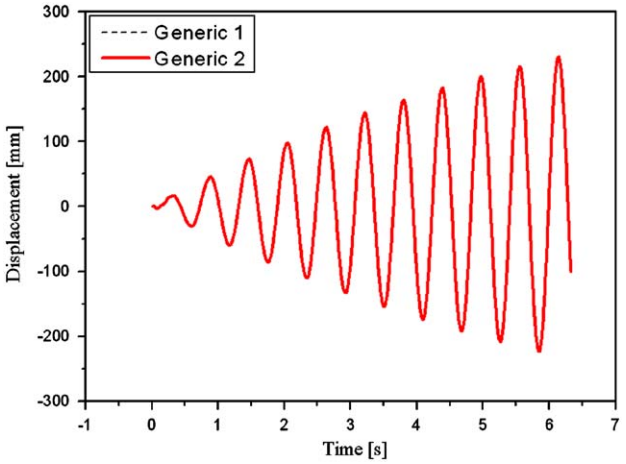

Fig. 17. Independent property of the generic damping model w.r.t. neighboring damping ratio: 1st mode; Generic 1 ($\zeta_1 = 1.2$, $\zeta_2 = 0.9$) and Generic 2 ($\zeta_1 = 1.2$, $\zeta_2 = 2.7$).

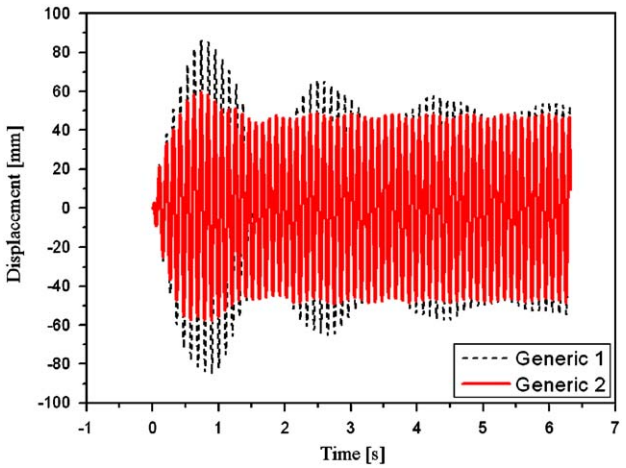

Fig. 18. Independent property of the generic damping model w.r.t. neighboring damping ratio: 2nd mode; Generic 1 ($\zeta_1 = 1.2$, $\zeta_2 = 0.9$) and Generic 2 ($\zeta_1 = 1.2$, $\zeta_2 = 2.7$).

Table 9
Optimized properties of the beam to match the natural frequency.

	Length (mm)	Width (mm)	Thickness (mm)	Density ($kg\,m^{-3}$)	Elastic modulus (MPa)
Standard	500	5.0	0.50	8000.0	210,000
Optimum	500	5.0	0.49	8108.0	205,130

Table 10
Optimized results of frequency matching.

Natural Frequency	Test (Hz)	Simulation (Hz)	
		Standard	Optimum
1st mode	1.85	1.67	1.84
2nd mode	10.19	10.47	10.18
3rd mode	26.84	29.32	26.81
4th mode	53.20	57.46	53.15
5th mode	88.60	94.97	88.79

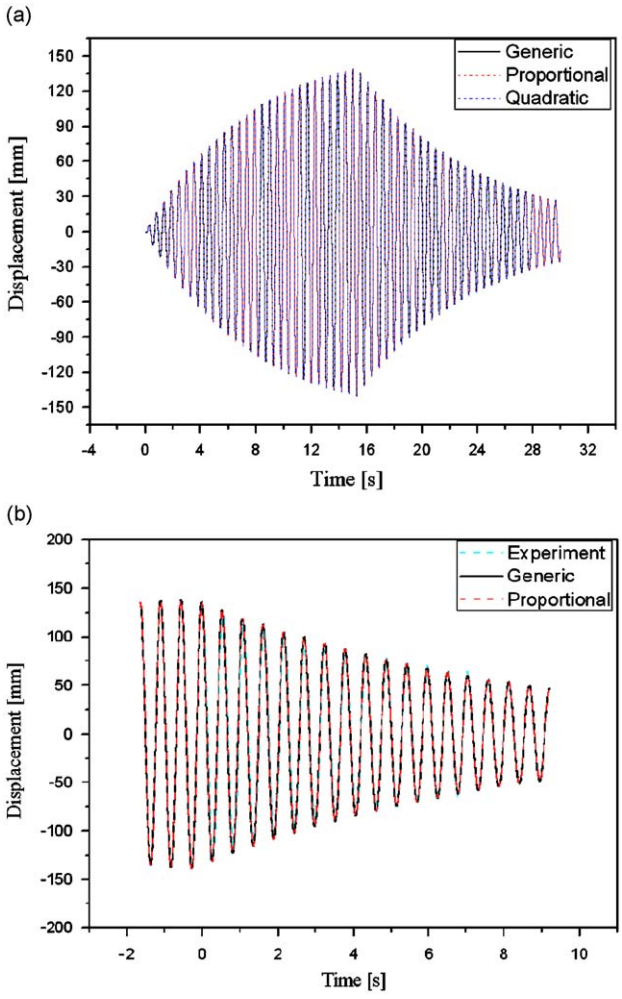

Fig. 19. Comparison of experiment and simulation: 1st mode: (a) comparison of three damping models and (b) comparison between simulation and experiment.

transformation is the transformation from the identified damping matrix in the modal domain to the general damping matrix in the physical reference domain using mode vectors. With the undamped natural modal matrix $\mathbf{\Phi}$, we can calculate the generic viscous damping matrix using orthogonal properties, as shown in Eq. (28), which describes the modal transformation of the generic damping matrix. Eq. (29) is an inverse modal transformation. We have

$$\mathbf{C}_g = \mathbf{\Phi}^{\mathrm{T}}\mathbf{C}\mathbf{\Phi} \tag{28}$$

$$\mathbf{C}=\mathbf{\Phi}^{-\mathrm{T}}\mathbf{C}_g\mathbf{\Phi}^{-1}=\mathbf{\Phi}^{-\mathrm{T}}\,\mathrm{diag}[2\zeta_n\omega_n]\mathbf{\Phi}^{-1} \tag{29}$$

where $n = 1,\ldots,m$ and $\mathrm{diag}[2\zeta_n\omega_n]$ is the diagonal matrix whose diagonal component is $2\zeta_n\omega_n$.

Using the mass normalization properties, we derive the inverse modal matrix such as

$$\mathbf{\Phi}^{\mathrm{T}}\mathbf{M}\mathbf{\Phi} = \mathbf{I} \tag{30}$$

$$\mathbf{\Phi}^{-1} = \mathbf{\Phi}^{\mathrm{T}}\mathbf{M}, \quad \mathbf{\Phi}^{-1} = \mathbf{\Phi}^{\mathrm{T}}\mathbf{M} \tag{31}$$

Substituting Eq. (31) into Eq. (29), the generic damping model can be calculated as

$$\mathbf{C} = \mathbf{M}\mathbf{\Phi}\,\mathrm{diag}[2\zeta_n\omega_n]\mathbf{\Phi}^{\mathrm{T}}\mathbf{M} \tag{32}$$

where $n = 1,\ldots,m$, $\mathbf{M}$ is a mass matrix, $\mathbf{\Phi}$ is a mode shape vector, and ζ_n, ω_n are critical damping ratio and the natural frequency derived from the modal parameter identification method, respectively.

The advantage of the generic damping model is to control the motion from low frequency to high frequency at the same time if every modal parameter could be extracted from the experiments. Each damping ratio is independent of neighboring

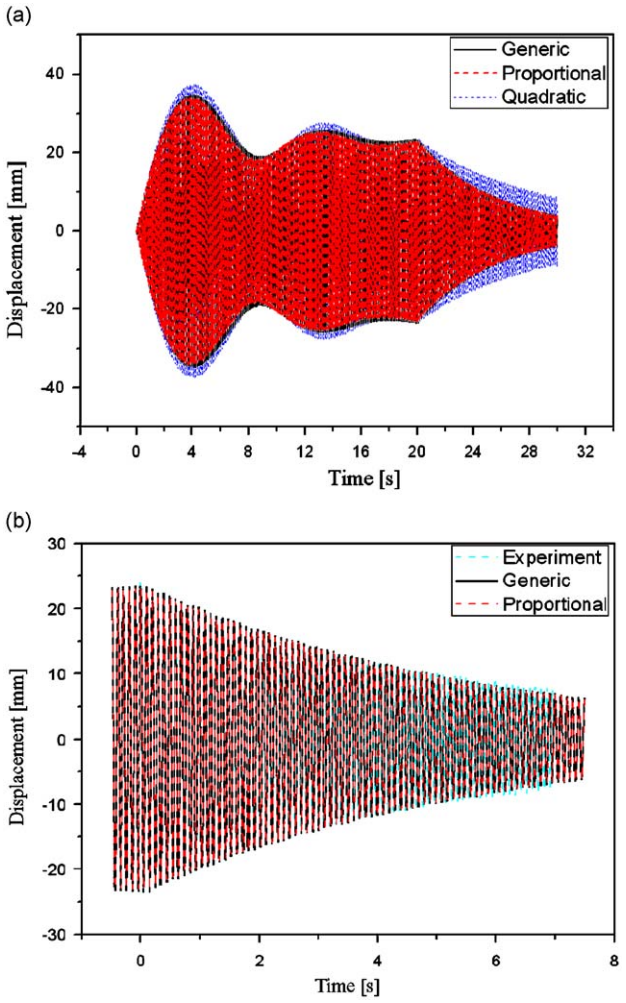

Fig. 20. Comparison of experiment and simulation: 2nd mode: (a) comparison of three damping models and (b) comparison between simulation and experiment.

modes. Therefore, it is possible to control the motion independently. In Table 8 and Figs. 17 and 18, we show that the property of generic damping is independent of the change in the neighboring damping ratio. For Generic 2 in Table 8, the damping ratio of the 2nd mode is increased to check the performance of the generic damping model. The simulation results are a transient response with harmonic base excitation. In Figs. 17 and 18, the change of the 2nd damping ratio cannot affect the 1st mode response. Thus, the generic damping model can control each damping ratio independently. It is impossible for the generic damping model to express the strong influence of air resistance forces that are not linear with respect to velocity, because the control parameter of generic damping in the frequency domain is the only damping ratio similar to the proportional damping model. More detail simulation conditions are given in Section 5.

5. Comparison of simulation and experiment

5.1. Matching process of natural frequencies

To the best of our knowledge, all researchers have focused on correlating their results with experiment at only the fundamental mode. The first mode with the lowest frequency is relatively easy to correlate. In higher order modes, the natural characteristics of the beam can strongly affect the response of the forced vibration behavior. Because heat-treated spring-steel is used, there is no guarantee that the natural properties of simulation coincide with those of experiment. Table 10 shows the difference in natural frequencies in the case of using standard properties of steel. Thus, a matching process was carried out to find proper material properties. The beam used in this study has 20 finite elements, 84 coordinates, and four constraint equations. The following design variables were selected: the width and height of each beam element and the elastic modulus, and density. The variance of these design variables was limited to within 10

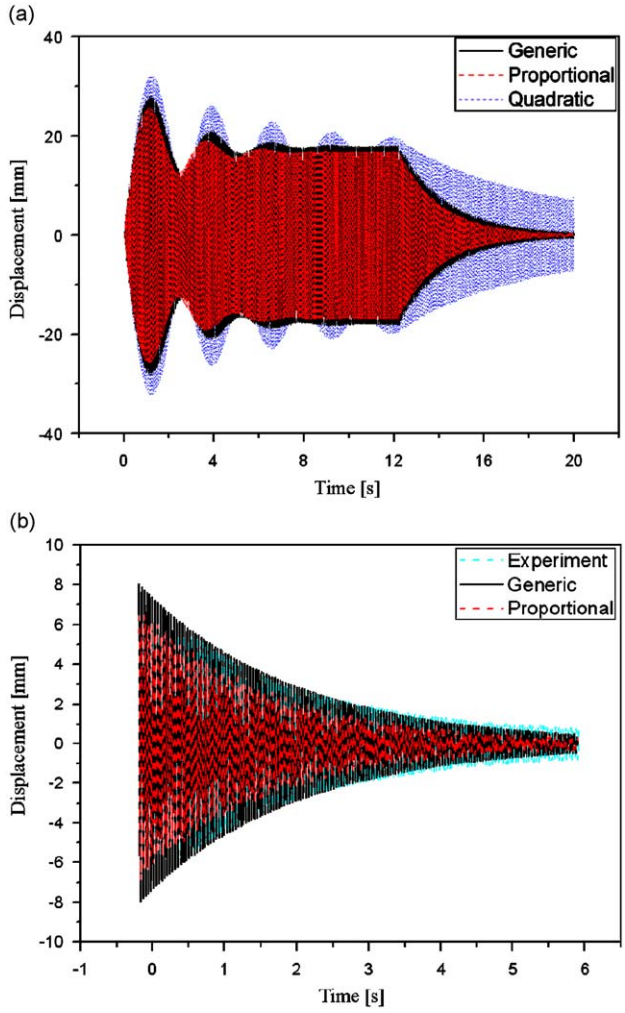

Fig. 21. Comparison of experiment and simulation: 3rd mode: (a) comparison of three damping models and (b) comparison between simulation and experiment.

percent. To correlate with natural characteristics, an objective function was chosen to minimize the residue of natural frequencies and modes from the 1st to the 5th mode. The resultant design variables are listed in Table 9, and Table 10 shows the optimized results. "Standard" in Table 9 means the material property of the general steel which is commonly used. "Optimum" means the optimized material property which has the optimum natural frequencies.

5.2. ANCF simulation results

Experiment and simulation with harmonic base excitation were carried out from the 1st mode to the 5th mode. Using the marker tracking method, the displacement of the beam was measured. In Figs. 19–23, "Generic" means the response of the generic damping model; "Proportional" (red dashed line) means the results of the proportional damping model; "Quadratic" (blue dashed line) means those of the quadratic damping model; and "Experiment" (blue dashed line with square) means the measured data of the experiment. In Fig. 19, the harmonic base excitation of the 1st mode at 1.85 Hz, was applied and the excitation is suddenly stopped after 15 s. The exponential decay behaviors of the three damping models and the experiment results were compared. The damping models all give good results compared to the experiment.

Fig. 20 shows the 2nd mode response, which has the same proportional, quadratic, and generic damping model used at the first mode. The excitation frequency is 10.19 Hz and the excitation was stopped at 20 s. The responses of the proportional and generic damping model are in good agreement with experiment. As previously mentioned, the proportional damping model can also control the first two mode behaviors due to the two control parameters. However, the quadratic damping model gave us the arbitrary response even 2nd mode in spite of the two control parameters. The equivalent damping ratio of the quadratic damping model is 0.16 percent, and this is the underestimated value compared to the experimental value of 0.28 percent.

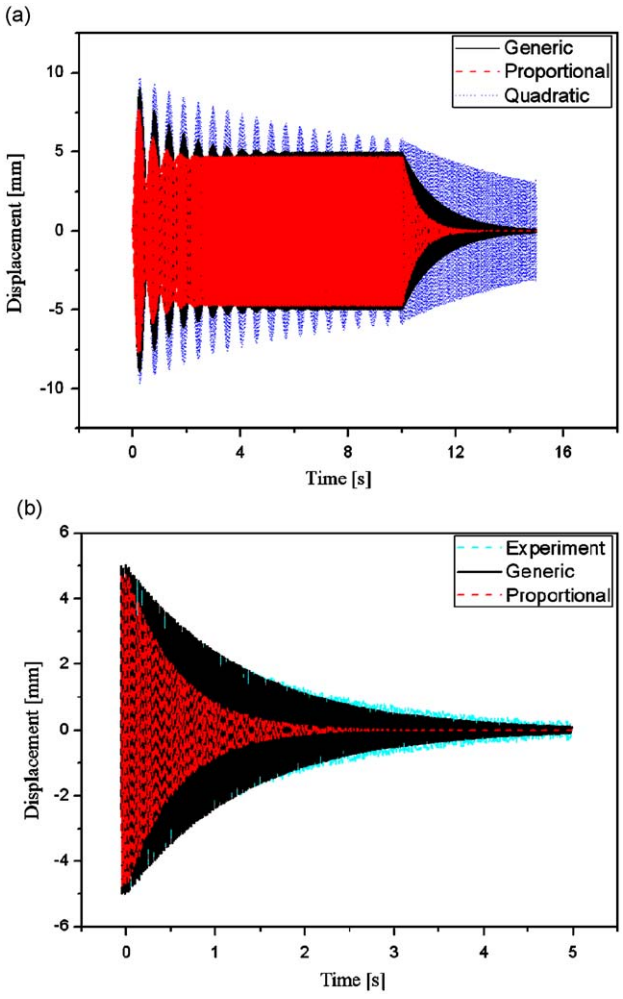

Fig. 22. Comparison of experiment and simulation: 4th mode: (a) comparison of three damping models and (b) comparison between simulation and experiment.

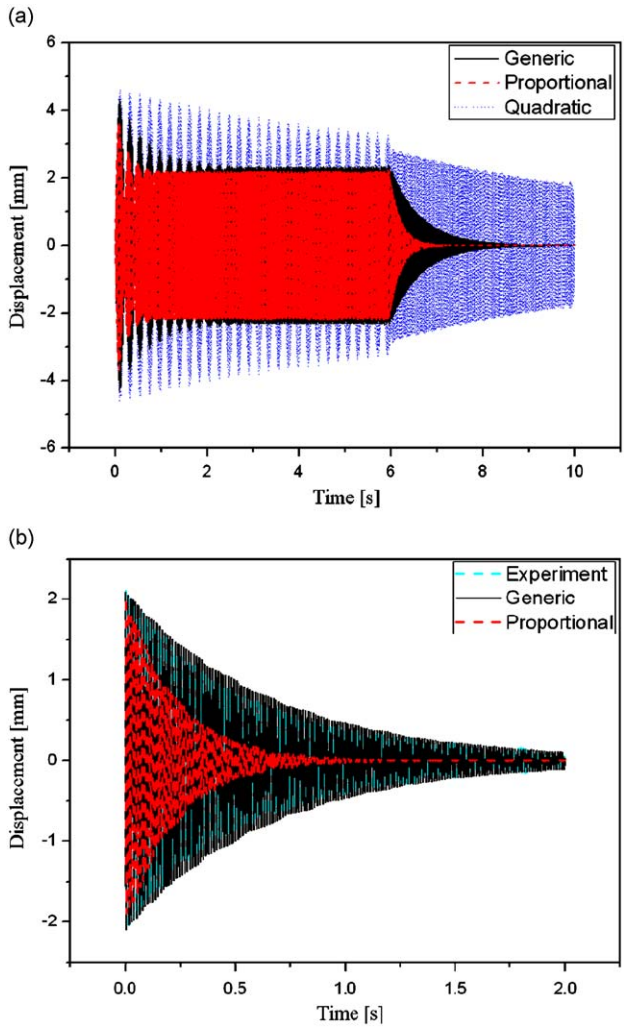

Fig. 23. Comparison of experiment and simulation: 5th mode: (a) comparison of three damping models and (b) comparison between simulation and experiment.

Table 11
Resultant damping ratio from experiment and simulation.

	Damping ratio of each mode (%)				
	1st	2nd	3rd	4th	5th
Experiment	1.00	0.28	0.28	0.23	0.300
Generic	1.00	0.28	0.28	0.23	0.300
Proportional	1.00	0.28	0.32	0.50	0.700
Quadratic	1.00	0.16	0.08	0.04	0.022

Fig. 21 shows the 3rd mode response, which has the same proportional, quadratic, and generic damping model used at the first mode. The same simulation process as the 1st mode was performed except the change of the excitation from 1.85 to 26.84 Hz. Because the steady state response was reached more quickly than the previous two simulations, the excitation was stopped at 12 s. The generic damping model also gave good results at this time. However, the proportional and quadratic damping models overestimate and underestimate that the damping ratio is 0.32 and 0.02 percent, respectively.

Figs. 22 and 23 show the 4th and 5th mode responses, respectively; these used the same damping models as the previous simulation. The simulation process is also the same except the excitation is at 53.20 and 94.97 Hz, respectively. The excitation was stopped at 10 and 6 s, respectively. The generic damping model also provided good results for these simulations. However, the proportional and quadratic damping models also overestimate and underestimate the damping

ratio at these simulations. The resultant estimated damping ratios are listed in Table 11. It is clear that proportional damping is prone to overestimating the damping ratio at the high frequency regions even though the estimated value is arbitrary because stiffness proportional damping dominates in high frequency regions and is prone to increase according to increment of the excitation frequency. In addition, quadratic damping is prone to underestimating the damping ratio at the high frequency regions. The reason is because the air-resistance force is relatively small in the high frequency regions in this example. In other words, the η_1 damping is dominant over all frequency ranges in this example, and the η_1 damping, which is independent of the excitation frequency, does not affect the damping forces according to the increase in the

Table 12
Quadratic parameters for equivalent damping ratio.

Mode	Damping ratio (ζ)	Equivalent quadratic parameters	
		η_1	η_2
1st	1.00	0.15	1.0E−4
2nd	0.28	0.31	6.0E−5
3rd	0.28	0.89	5.0E−5
4th	0.23	1.46	5.0E−5
5th	0.30	3.00	5.0E−5

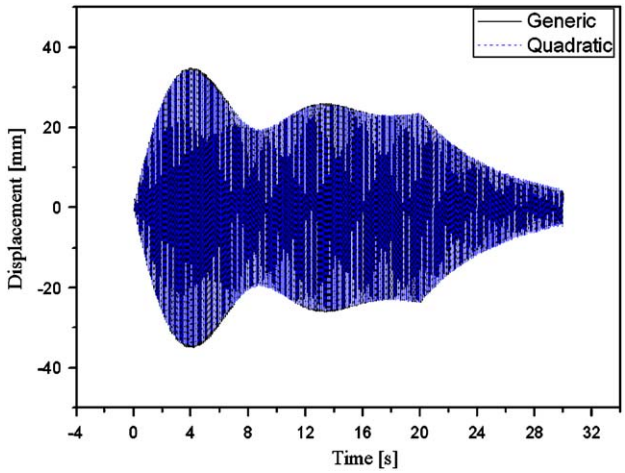

Fig. 24. Individual quadratic damping model: 2nd mode; Generic damping ($\zeta_2 = 0.28$) and Quadratic damping ($\eta_1 = 0.31$, $\eta_2 = 6.0\text{E} - 5$).

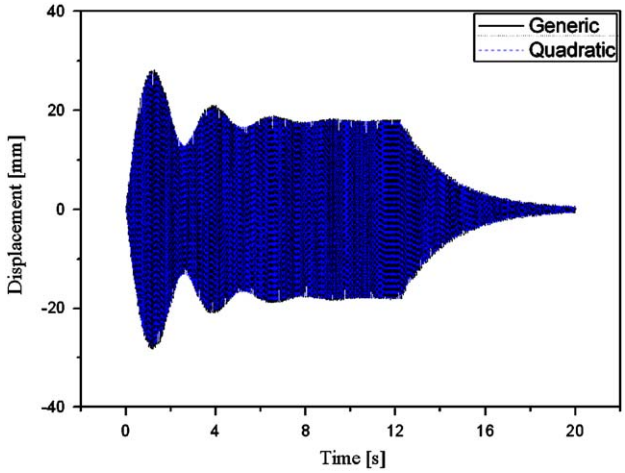

Fig. 25. Individual quadratic damping model: 3rd mode; Generic damping ($\zeta_3 = 0.28$) and Quadratic damping ($\eta_1 = 0.89$, $\eta_2 = 5.0\text{E} - 5$).

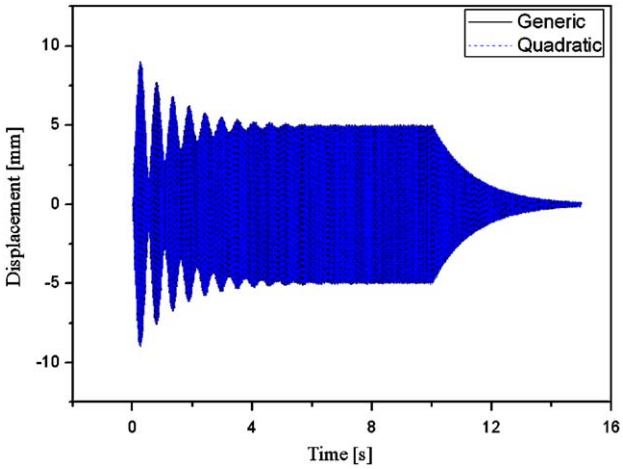

Fig. 26. Individual quadratic damping model: 4th mode; Generic damping ($\zeta_4 = 0.23$) and Quadratic damping ($\eta_1 = 1.46$, $\eta_2 = 5.0\text{E}-5$).

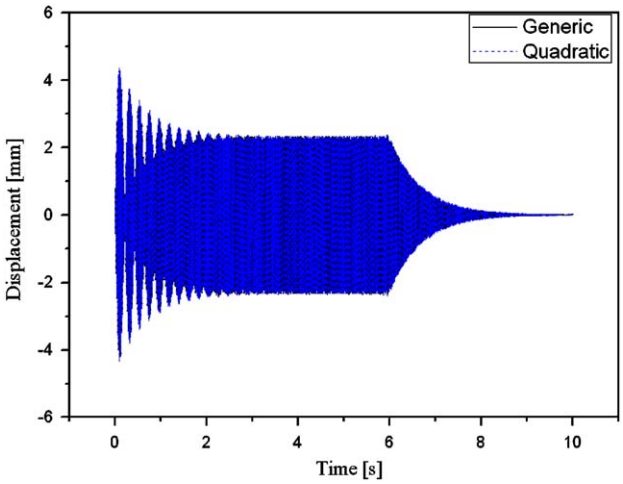

Fig. 27. Individual quadratic damping model: 5th mode; Generic damping ($\zeta_5 = 0.30$) and Quadratic damping ($\eta_1 = 3.00$, $\eta_2 = 5.0\text{E}-5$).

excitation frequency. Thus, the quadratic damping model tends to underestimate the damping ratio in high frequency regions.

To correlate high frequency behavior with the quadratic damping model, each damping model per mode is needed, as previously explained. The identified quadratic damping model, which is explained in Section 4, is listed in Table 12. If the quadratic damping model with the parameters in Table 12 is used at each excitation frequency, well-correlated results can be found, as shown in Figs. 24–27.

6. Conclusion

The main goal of this study is to develop a proper damping model for the absolute nodal coordinate formulation. In previous studies, the proportional damping matrix was widely used for simplicity, and quadratic damping was used to express hydrodynamic drag force. However, these models cannot control high frequency behavior with only one or two damping matrices.

We propose a frequency-dependent generic damping model. Our damping model describes the response of the entire frequency range as a single damping model, and is easier to use than the individual quadratic damping model. In addition, our model leads to get more accurate correlation results because it directly uses the modal parameters of each mode obtained from experiments, and can present exact high frequency behaviors simultaneously. We also showed that the traditional modal superposition theory can be applied to a flexible beam undergoing large deformation with the absolute nodal coordinate formulation, in which nodal displacements and slopes are defined in an inertial reference frame.

A new experimental modal testing method was presented which uses the concept of global parameters. Traditional modal testing is difficult to apply to large deformation problems due to the poor accuracy of the experimental results. Using our modal testing method, the displacement of a flexible beam was measured to the 5th mode (89 Hz). Finally, through comparisons with ANCF simulations, the strengths and weaknesses of each external damping model were discussed. It was shown that the common drawbacks of proportional and quadratic damping are complemented by the proposed generic damping model.

Acknowledgment

This work was supported by the Korea Science and Engineering Foundation (KOSEF) grant funded by the Korea government (MEST) (NO. R01-2008-000-20373-0).

References

[1] A.H. Nayfeh, *Linear and Nonlinear Structural Mechanics*, Wiley, New York, 2004.
[2] S.H. Crandall, The role of damping in vibration theory, *Journal of Sound and Vibration* 11 (1) (1970) 3–18 (IN1).
[3] M.A.V. Rangacharyulu, B.V. Dasarathy, Non-linear systems with quadratic and cubic damping: an analytical approach, *Journal of Sound and Vibration* 38 (1) (1975) 9–13.
[4] J.P. Bandstra, Comparison of equivalent viscous damping and nonlinear damping in discrete and continuous vibrating systems, *Journal of Vibration, Acoustics, Stress and Reliability in Design* 105 (1983) 382–392.
[5] W.E. Bakers, W.E. Woolam, D. Young, Air and internal damping of thin cantilever beams, *International Journal of Mechanical Science* 9 (1967) 743–766.
[6] A.A. Shabana, Flexible multibody dynamics: review of past and recent developments, *Multibody System Dynamics* 1 (1997) 189–222.
[7] A.A. Shabana, *Dynamics of Multibody Systems*, third ed., Cambridge University Press, Cambridge, 2005.
[8] Y. Takahashi, N. Shimizu, K. Suzuki, Introduction of damping matrix into absolute coordinate formulation, *Proceedings of the Asian Conference on Multibody Dynamics*, Iwaki, Fikushima, 2002, pp. 33–40.
[9] W.S. Yoo, J.H. Lee, J.H. Sohn, S.J. Park, O. Dmitrochenko, D. Pogorelov, Large oscillation of a thin cantilever beam: physical experiments and simulation, *Nonlinear Dynamics* 34 (2003) 3–29.
[10] W.S. Yoo, J.H. Lee, S.J. Park, J.H. Sohn, D. Pogorelov, O. Dmitrochenko, Large deflection analysis of a thin plate: computer simulations and experiments, *Multibody System Dynamics* 11 (2004) 185–208.
[11] D. Garcia-Vallejo, J. Valverde, J. Dominguez, An internal damping model for the absolute nodal coordinate formulation, *Nonlinear Dynamics* 42 (2005) 347–369.
[12] D.J. Ewins, *Modal Testing: Theory, Practice and Application*, second ed., Research Studies Press Ltd., 2000.
[13] K.G. McConnell, *Vibration Testing: Theory and Practice*, Wiley, New York, 1995.
[14] M. Berzeri, A.A. Shabana, Development of simple models for the elastic forces in the absolute nodal coordinate formulation, *Journal of Sound and Vibration* 235 (4) (2000) 539–565.
[15] B. Buckham, M. Hahon, M. Seto, X. Zhao, C. Lambert, Dynamics and control of a towed underwater vehicle system, part I: model development, *Ocean Engineering* 30 (2003) 453–470.